Near-navigation-grade interferometric fiber optic gyroscope with an integrated optical chip

Kejun Shang (尚克军)[1,2], Ming Lei (雷 明)[2,*], Qiang Xiang (向 强)[2], Yonglin Na (那永林)[2], Lizhe Zhang (张丽哲)[2], and Huaiyong Yu (于怀勇)[2]

[1]*School of Automation, Beijing Institute of Technology, Beijing 100081, China*
[2]*State Key Laboratory of Inertial Technology, Beijing Institute of Automatic Control Equipment, Beijing 100074, China*
**Corresponding author: leiming1998@yeah.net*

Received June 7, 2020; accepted August 11, 2020; posted online September 25, 2020

We present a near-navigation-grade interferometric fiber optic gyroscope (IFOG) based on an integrated optical chip. The chip comprises a light source, a photodiode, and a 3 dB coupler within an area of 48 mm^2. By interrogating with an integrated optical modulator and a small-diameter sensing coil, the IFOG is realized. This allows for a significant reduction in size, weight, power consumption, and cost. Preliminary performance data of a gyro prototype exhibits 0.018 deg/h bias instability.

Keywords: gyroscopes; fiber optics; fiber optics sensors; integrated optics.
doi: 10.3788/COL202018.120601.

Interferometric fiber optic gyroscopes (IFOGs) were developed for decades before their performance became sufficient for commercial use[1–3]. Today, IFOGs are rapidly increasing in performance while having reduced size, weight, and cost[4,5]. An IFOG is comprised of a passive sensing coil, discrete optical components [superluminescent diode (SLD), photodiode (PD), coupler, polarizer, Y-junction, phase modulator (PM)] packaged with fiber pigtails, and a signal processing circuit. This not only results in a large footprint but also degrades the IFOG's performance due to reflection and polarization misalignments at the connection points.

Multi-functional integrated optical modulator chips (IOMCs), which include a polarizer, Y-junction, and PM for closed-loop operation, have been widely used in IFOGs[6–8]. To reduce the size of the sensing coil, it can be integrated into an optics chip by ultra-low-loss waveguide coil technology[9–12]. However, the precision current of IFOGs is usually too low to meet high-performance requirements. To maintain high sensitivity over long fiber lengths and improve the performance of miniaturized IFOGs, thin, small-diameter, polarization-maintaining fiber technology has been developed[13,14]. Cladding fibers have been reduced to ∼100 μm diameters, and mini-coil diameters are now as small as 20 mm[15]. Even the use of photonic crystal fibers can significantly reduce the size of the sensing coil[16]. Moreover, in order to miniaturize the signal processing circuit, an analog-to-digital converter (ADC), digital-to-analog converter (DAC), and field-programmable gate array (FPGA) can be integrated into a chip[17,18]. However, other discrete optical components, like SLDs, PDs, and couplers, have not been similarly miniaturized.

Using discrete optical components not only increases the size of IFOGs but also results in parasitic reflections, which increase insertion losses at fusing points[19]. The idea of integrating discrete optical components into an optical chip for use in an IFOG was introduced early in 1990 and can be called an "optical engine". With the development of monolithically integrated optical components and waveguide circuit techniques, many researchers have integrated discrete optical components into integrated optical chips (IOCs). These IOCs have some outstanding size, weight, power consumption, and cost (SWaP-C) characteristics and are used in sensors[20], optical communications[21], and ultra-stable atomic clocks[22]. Hybrid integration of IFOG was proposed by Bischel for use in harsh environments[23]; however, the IOCs are too large for use in compact IFOGs. Tran *et al.* reported the first chip-scale IOC comprised of a light source, three PDs, two PMs, and two 3 dB couplers based on photonics integration technology. It fit within an area of 4.5 mm^2, but the precision of the IFOG was very low at roughly 2 deg/s in rotational measurement[24]. In 2019, a polarizer and two Y-branches were integrated in an IOC to reduce the cost of an open-loop IFOG[25]. It obtained a bias drift of 0.048 deg/h. However, major discrete optical components, such as the SLD and PD, were not integrated into the IOC.

An IOC integrating an SLD, PD, and coupler is proposed for IFOG application in this work. We describe the design of the IOC, sample fabrication, and testing of the optical power, linewidth, and central wavelength. An IFOG prototype based on IOC was assembled, and the bias instability and scale factor were tested under coils of different length. The bias instability was low at 0.018 deg/h, which demonstrates that the primary performance of the IOC can satisfy the requirements of a near-navigation-grade IFOG.

The schematic configuration of the IFOG based on IOC is shown in Fig. 1. The IOC includes the following components: (1) an incoherent light source SLD; (2) a photodetector PD; (3) a Y-branch Y1. Due to the serious impact of asymmetric spatial modes on the IFOG's

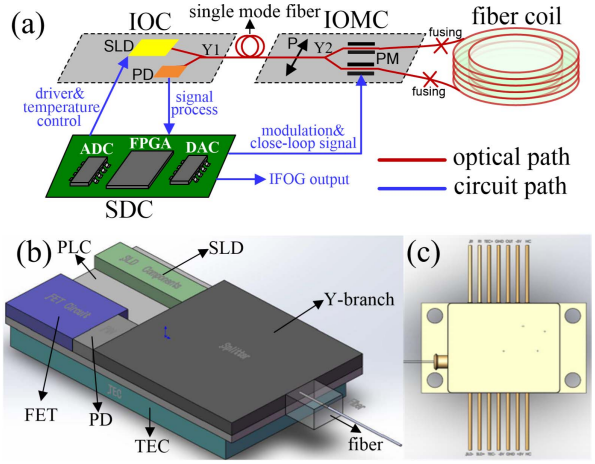

Fig. 1. (a) Schematic illustration of the IFOG based on an IOC. IOC, integrated optical chip; IOMC, integrated optical modulator chip; SDC, signal detection circuit; SLD, superluminescent diode; PD, photodiode; Y1/Y2, Y-branch; P, polarizer; PM, phase modulator; ADC/DAC, analog-to-digital/digital-to-analog converter; FPGA, field-programmable gate array. (b) Configuration of the IOC layout and (c) IOC package structure.

performance, an IOMC circuit was adopted, which includes the following components: (1) a polarizer to minimize polarization drift; (2) a Y-branch Y2 to divide the wave into clockwise (CW) and counter-CW (CCW) travel; and (3) a PM to achieve closed-loop operation. The fiber coil in Fig. 1 is typically a coil of thin-cladding polarization-maintaining fiber, which has a length of hundreds of meters to ensure the IFOG's accuracy. A signal detection circuit (SDC) based on ADC, DAC, and FPGA is used to realize high-resolution analog/digital measurement of the rotation rate, as well as to act as the driver and temperature control for the SLD.

To improve the manufacturability and performance of the IFOG while reducing its cost, a multiple optical component packaging technology was used to provide electrical interconnection and light coupling between the optical components to ensure that the optical device operates optimally. In addition, a thermo-electric cooler (TEC) was used to maintain efficient thermal expansion between the SLD and submounts, which can result in significantly increased lifetime.

An epoxy attachment is generally considered the lowest-cost attachment process for building photonic devices. It is commonly used in photonic device proof-of-concept demonstration builds and early prototype builds because of its ease of use, low cost, and availability. Here, all of the optical components, including the TEC, SLD, field effect transistor (FET), and PD were attached by epoxy to the substrate to ensure the module's performance and reliability. The configuration layout of the IOC is illustrated in Fig. 1(b).

By designing a large-pitch silicon dioxide planar optical waveguide circuit (PLC)-type Y-branch chip, sufficient space is provided for the integration of the SLD and PD. The SLD is suitable for use with gyroscopes due to its large operational bandwidth. To expand its bandwidth, we adopted the dual quantum well design to expand the bandwidth of the III-V gain medium. An optical surface-matching SLD chip was mounted into a PLC through chip-to-chip coupling techniques. The main aim is to realize low-loss, high-integration coupling between the SLD chip and Y-branch chip. To increase the coupling efficiency and improve the signal-to-noise ratio (SNR) of the IFOG, a tapered mode conversion waveguide was optimized, and high-precision passive alignment was used. The process tolerance requirements are all within 1 μm because the sizes of the chip waveguide end-faces are all in the order of micrometers.

The next chip in the IOC is the PD chip. InGaAs was bonded to an InP substrate by a wafer bonding process with low dark current, high responsivity, and high reliability. The p-n junction in the positive-intrinsic-negative (PIN) structure converts photons into current. The absorbed photons make electron-hole pairs in the depletion region, which is one of the key subcomponent technologies required to manufacture etched metalized micro-mirrors that redirect light out of the waveguide and into the surface-mounted PD chip. Moreover, an FET circuit is used to convert the photo-current to voltage.

The Y-branch Y1 is a 3 dB passive waveguide coupler made with doped SiO_2, which is used to direct 50% of the light propagating in the waveguide into the SLD and PD arrays that are surface mounted on the chip. Non-equal splitting of the coupler can cause increased backscattering and Kerr noise[26,27]. For Y-branch structures manufactured by doping with SiO_2, the Y-branch structure simulation design, process parameter exploration, and chip end-face coupling analysis are required to achieve high uniformity of the splitting ratio.

The IOC also contains a coupling-out structure, which provides light coupling into and out of the sensing coil. A semi-automated pigtailing process for the PM fiber was developed that uses a micro-machined polish-cut process with a dicing saw to fabricate the end-face. Then, automatic coupling alignment was realized to improve the coupling efficiency between the fiber and the IOC waveguide. In order to suppress back-reflection noise, the surface of the waveguide was optimized to a tilted angle. Eventually, suitable curing glue was used to strengthen the coupling package structure, significantly improving the strength and reliability of the IOC.

The IOC, with a small size of 8 mm × 6 mm, was mounted on a TEC to maintain an emission wavelength sufficient for proper operation. All these components stand within a 26 mm × 12 mm metallic package, which is interfaced and wire-bonded to allow electrical contact with 14 electrical pins and a fiber pigtail that isolates the package from external interference. The package structure of the IOC is shown in Fig. 1(c).

Another key enabling component for an IFOG is the IOMC, which has multiple functions and is typically fabricated from lithium niobate. The lithium niobate

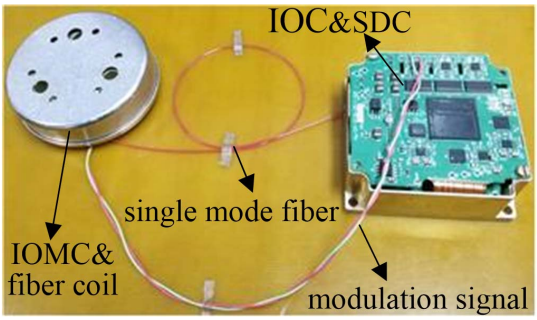

Fig. 2. IFOG prototype based on an IOC.

quad-PM array chip uses previously developed state-of-the-art IOC chip design and fabrication techniques, primarily inductively coupled plasma (ICP) etching, proton exchange, and annealing. Polarizer P filters out cross-coupled erroneous signals in the light returning from the sensing coil by eliminating the transverse magnetic (TM) mode with a high polarization extinction ratio (PER). Y-branch Y2 is a 3 dB passive waveguide coupler based on a common substrate of lithium niobate. The physical size of the packaged IOMC is 20 mm × 10 mm.

Because of the limited rejection of the common base waveguide that acts as the spatial filter in the IOMC, a single-mode fiber (that can be seen as an absorber or a filter) is used to eliminate the anti-symmetrical mode radiating from the Y-junction, thereby ensuring optic reciprocity and improving the IFOG's performance.

According to the integrated optical design and fabrication techniques shown in Fig. 2, an IOC with an effective package was successfully processed. An experiment was set up to test the IOC, which was driven at a constant 100 mA current and a controlled constant temperature. The properties of optical power, central wavelength, linewidth, extinction ratio, responsivity, 3 dB bandwidth, noise voltage, and power consumption (−40°C–60°C) were measured and are listed in Table 1.

An IFOG prototype based on the pigtailed IOC was successfully fabricated, as shown in Fig. 2. The sensitive head consisted of an IOMC and a fiber coil, which was placed inside magnetic shields to reduce the ambient magnetic field. The IOC and SDC were assembled into a designed base structure and connected to the sensitive head by a single-mode fiber and a modulation signal cable.

Table 1. Measured Results of the IOC

IOC	Performances	Values
SLD	Optical power (μW)	149
	Central wavelength (nm)	1300.21
	Linewidth (nm)	41
	Extinction ratio (dB)	0.3
PD	Responsivity (A/W)	0.88
	3 dB bandwidth (MHz)	6
	Noise voltage (mV)	0.49
Coupler	Splitting ratio	50.6:49.4
Power consumption (W, −40°C to 60°C)		1.26

Table 2. Measured Results of the IFOGs Based on an IOC

IFOG	#1	#2	#3
Average diameter (cm)	3.8	4.5	4.5
Fiber length (m)	270	500	500
Measured scale factor	17,000	37,000	37,000
Measured in-run bias instability (deg/h)	0.13	0.018	0.0073
ARW (deg/$h^{1/2}$)	0.1	0.014	0.0033

To compare IOC performances for IFOG application, sensing coils with different lengths and diameters were made of thin-clad polarization-maintaining fiber with dimensions of 80/135 μm. The detailed configurations of the two IFOGs are listed in Table 2. Note that IFOG #2 has a larger scale factor than IFOG #1. This resulted in better performance for IFOG #2. Also listed in Table 2 are the measured performance attributes of the two IFOGs.

The scale factor of the IFOGs was calibrated on a precision rate table at room temperature. The in-run bias instability of the two IFOGs was obtained via Allan variance analyses of the noise data collected, as shown in Fig. 3. Bias instability of IFOG #2 with a 500 m fiber coil and an IOC was 0.018 deg/h, and the angular random walk (ARW) was estimated to be 0.014 deg/$h^{1/2}$. To compare the performances, an IFOG with discrete optical components (IFOG #3) and the same size and length of fiber loops as IFOG #2 was built; the detailed configuration is given in Table 2. The static test results are shown in Fig. 3. The bias instability and ARW of IFOG #3 were 0.0073 deg/h and 0.0033 deg/$h^{1/2}$, respectively, which are both obviously better than those of IFOG #2.

The biases of the IFOGs with IOC and discrete optical components were measured over a temperature range of

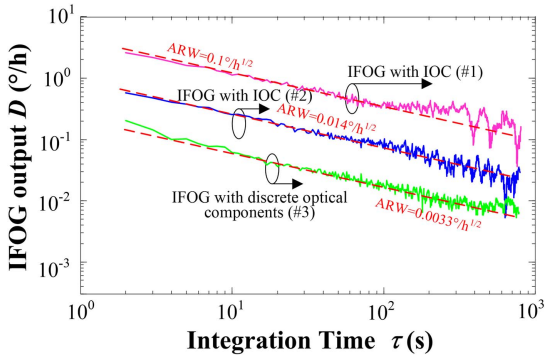

Fig. 3. Bias instabilities of IFOGs with IOC and discrete optical components.

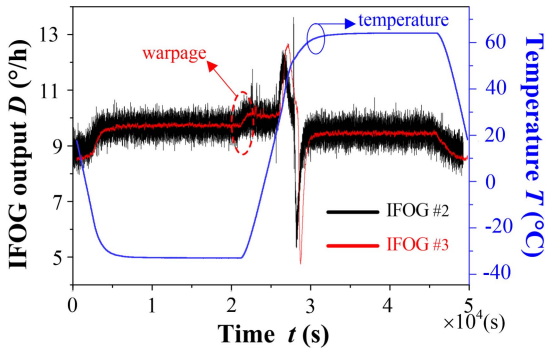

Fig. 4. IFOG bias versus temperature.

−40°C to 60°C at a change rate of 1°C/min. The test results in relation to temperature are shown in Fig. 4.

As can be seen from Fig. 4, the background noise of IFOG #2 was obviously greater than that of IFOG #3, leading to greater bias instability and ARW. However, as the temperature changed, the bias-drift characteristic of the IFOG with IOC was the same as the one with discrete optical components and was caused by the temperature-related Shupe effect. Furthermore, the same warpages occurred when the temperature change was non-uniform. By sampling ambient temperature changes and performing gyro zero-drift compensation, the IFOG's output drift can be significantly reduced. The related compensation technology is very mature in IFOG signal processing.

The test results were fully comparatively analyzed. The performance of the IFOG with IOC was mainly limited by photon, electron, and magnetic cross-coupling due to the chip-scale size, which caused a low SNR and poor accuracy.

In conclusion, we have proposed and demonstrated a near-navigation-grade IFOG based on IOC. It allows for a reduction in the SWaP-C of navigation-grade gyros used for engineering. Future work will conduct more characterization of the circuit design to suppress noise and limitations, which will be beneficial for improving the next generation of IFOGs. Furthermore, with proper integration modifications, an IOC and an IOMC will be integrated into a single chip. Technologies that eliminate the anti-symmetrical mode radiating from the Y-branch should be considered to ensure reciprocity and improve IFOG performance. We will report the results of this ongoing work in a future publication.

The authors gratefully acknowledge the useful suggestions given by Daoxin Dai, Yaocheng Shi, and Ming Zhang of Zhejiang University.

References

1. H. C. Lefevre, *The Fiber-optic Gyroscope*, 2nd ed. (Artech House, 2014).
2. J. Oliver, J. Navig. **9**, 3 (2007).
3. Z. Pan, C. Zhang, C. Xie, Y. Zheng, H. Li, J. Tang, and J. Liu, Chin. Opt. Lett. **16**, 040601 (2018).
4. J. Scheuer, Opt. Lett. **34**, 1630 (2009).
5. R. A. Bergh, L. Arnesen, and C. Herdman, Proc. SPIE **9852**, 98520E (2016).
6. N. Liu, Y. Niu, L. Feng, H. Jiao, and X. Wang, Chin. Opt. Lett. **16**, 010608 (2018).
7. R. Luo, Y. Li, and S. Deng, Opt. Lett. **43**, 4 (2018).
8. B. Wu, Y. Yu, and X. Zhang, Sci. Rep. **9**, 12946 (2019).
9. P. P. Khial, A. D. White, and A. Hajimiri, Nat. Photon. **12**, 671 (2018).
10. D. Blumenthal, in *IEEE Photonics Conference* (2016), p. 347.
11. B. Wu, Y. Yu, J. Xiong, and X. Zhang, Sci. Rep. **8**, 8766 (2018).
12. S. Gundavarapu, M. Belt, T. Huffman, M. A. Tran, T. Komljenovic, J. E. Bowers, and D. J. Blumenthal, Proc. SPIE **10323**, 103231A (2017).
13. W. Li, Y. Gao, and L. Tong. IEEE Photon. Tech. Lett. **31**, 18 (2019).
14. J. Daenicke, M. Lämmlein, F. Steinhübl, and D. W. Schubert, e-Polymers **19**, 330 (2019).
15. J. Jin, J. He, K. Ma, and L. Kong, in *6th IEEE International Symposium on Inertial Sensors and Systems* (2019).
16. T. Lei, H. Zhang, and Y. Dong, Opt. Lett. **41**, 729 (2016).
17. C. Croker, G. W. Keith, and N. G. Tarleton, European Patent EP 2,762,833 (August 6, 2019).
18. D. Olaf, D. Georg, K. Stefan, M. Tim, V. Sven, and Z. Steffen, Sensors **17**, 567 (2017).
19. R. Bi, L. Miao, T. Huang, G. Ying, S. Che, and X. Shu, Sensors **19**, 2851 (2019).
20. K. Yang, D. Oh, S. Lee, and Q. Yang, Nat. Photon. **12**, 5 (2017).
21. B. Chen, H. Wu, C. Xin, D. Dai, and L. Tong, Nat. Commun. **8**, 20 (2017).
22. L. Zachary, M. Vincent, and D. Tara, Optica **6**, 5 (2019).
23. W. Bischel, M. Kouchnir, and M. Bitter, Proc. SPIE **8164**, 81640Q (2011).
24. M. A. Tran, T. Komljenovic, J. C. Hulme, M. J. Kennedy, D. J. Blumenthal, and J. E. Bowers, Opt. Express **25**, 4 (2017).
25. L. Wang, D. Halstead, and T. Monte, in *IEEE International Symposium on Inertial Sensors and Systems* (2019).
26. S. Srinivasan, R. Moreira, D. Blumenthal, and J. Bowers, Opt. Express **22**, 24988 (2014).
27. R. A. Bergh, H. Lefevre, and H. Shaw, Opt. Lett. **7**, 6 (1982).